BNL-107350-2015-JA

Characterization of One-Dimensional Molecular Chains of 4,4'-Biphenyl Diisocyanide on Au(111) by Scanning Tunneling Microscopy

Jing Zhou,[1*] Yan Li,[2] Percy Zahl,[3] Peter Sutter,[3] Dario J. Stacchiola,[4] and Michael G. White[1,4]

[1]*Department of Chemistry, University of Stony Brook, Stony Brook, New York 11794*

[2]*Computational Science Center, Brookhaven National Laboratory, Upton, New York 11973*

[3]*Center for Functional Nanomaterials, Brookhaven National Laboratory, Upton, New York 11973*

[4]*Chemistry Department, Brookhaven National Laboratory, Upton, New York 11973*

Abstract

The morphology and electronic structure of vapor deposited 4,4'- biphenyldiisocyanide (BPDI) on a Au(111) surface was investigated using variable-temperature scanning tunneling microscopy (STM). When deposited at room temperature, BPDI molecules form one-dimensional molecular chains similar to that recently observed for the structurally related 1,4-phenyl diisocyanide (PDI). Compared to PDI, the longer periodicity for the BPDI molecular chains is consistent with the addition of a second phenyl ring and supports a structural model in which the BPDI molecules lie parallel to the surface and interconnected by Au-adatoms. The molecular chains are mostly aligned along the $[1\bar{1}0]$ direction of the Au(111) substrate, but exhibit frequent changes in angle that are consistent with directions between *fcc* and *hcp* three-fold hollow sites. Dispersion-corrected DFT calculations for one-dimensional chains of BPDI molecules bound end-to-end via their isocyanide groups to Au-adatoms reproduce the observed periodicity of the chains and show that this morphology is energetically favored over upright binding with one free –NC group. The spatially resolved conductance (dI/dV) map for BPDI on

*Present address: Applied Materials, Santa Clara, CA

Au(111) exhibits a feature centered at -0.67 eV below the Fermi level which delocalized along the chain with maxima at the Au-adatom and biphenyl positions. This occupied resonant feature is close to that previously observed for the PDI in both photoemission and conductance measurements and is attributed to an occupied interfacial state resulting from BPDI-Au interactions.

1. Introduction

By spontaneously assembling into densely packed and well-ordered structures, self-assembled monolayers (SAMs) provide a convenient, flexible way to modify the surface properties of metals and have been proposed for a number of applications such as molecular electronic devices.[1-3] Aromatic isocyanides have attracted widespread interest for this application as the N≡C triple bond is expected to effectively connect $p\pi$ orbitals of the aromatic moiety with $d\pi$ orbitals of the gold surface. These qualitative expectations are supported by measurements[4-8] and theoretical calculations[9-12] which suggest that molecules with terminal isocyanide groups exhibit higher conductance when bound to a Au surface than the same molecule with a terminal thiol group. Other studies suggest that isocyanide molecules have larger HOMO-LUMO gaps and are therefore expected to be poorer conductors than the corresponding thiol molecules.[13] A similar conclusion was reached from molecular break-junction studies of aromatic thiols versus aromatic isocyanides.[14] This is further supported by advanced GW calculations,[15,16] which show that the energies between phenylene diisocyanide levels and the Fermi level of Au(111) are much larger than that predicted by conventional density functional theory (DFT).[11,12] Overall, no consensus has been reached about the electronic structure of adsorbed aromatic isocyanides on gold, or how it is affected by coverage and surface morphology. Such information is crucial for developing a fundamental understanding of the diisocyanide-gold interactions that are ultimately responsible for the macroscopic conductance properties of diisocyanide SAMs on metal surfaces.

Previous studies of aromatic diisocyanide SAMs on a Au(111) surface prepared from solutions demonstrated that the diisocyanide molecules bind to the Au surface through a single Au–C bond with a near vertical geometry.[5-10] Support for the upright bonding geometry was based on infrared spectroscopy and sum frequency generation measurements which exhibited the

presence of two N≡C stretching frequencies corresponding to a free –NC group and a –NC group bonded to the surface which has a higher frequency. Polarization-dependent photoemission studies of 4,4′-biphenyldiisocyanide (BPDI) SAMs on Au(111) also concluded that the terminal layer of BPDI molecules were oriented in an upright geometry.[13] By contrast, recent scanning tunneling microscopy (STM) experiments showed that 1,4-phenyldiisocyanide (PDI) deposited from the vapor onto a Au(111) surface at room temperature form one-dimensional (1-D) molecular chain structures.[17,18] The proposed adsorption model for this molecular chain involves alternating PDI molecules and Au adatoms, i.e., a repeating [-PDI-Au-] monomer unit. In this structure, the PDI molecules lie flat on the surface and are bonded at each end to Au-adatoms, which originate from step edges or the Au(111) surface reconstruction. The participation of Au-adatoms in the formation of 1-D molecular chains is similar to that proposed for the binding of alkane thiolates (RS-Au-SR dimers) in the so-called "striped phases" on the Au(111) surface.[19-23]

In a related study, Zhou, et al., examined the temperature-dependent surface morphology and electronic structure of PDI/Au(111) surfaces using a combination of variable-temperature STM and two-photon photoemission (2PPE) spectroscopy.[24] It was found that the PDI molecules vapor-deposited at low temperature formed disordered islands or very short chain segments at step edges. As the surface was heated to room temperature, the disordered islands disappeared and the PDI molecules self-organized into 1-D molecular chains. 2PPE measurements on similarly prepared PDI/Au(111) surfaces showed that the dramatic change in morphology was also accompanied by a large drop in the work function and the formation of a new occupied electronic state (-0.88 eV below E_F). The occupied state was attributed to the hybridization of PDI molecular levels with the valence orbitals of Au-adatoms. STM images were also obtained at higher PDI coverage (0.1-0.2 ML), where long molecular chains were

found to grow uniformly over the Au terraces, but retained their original orientation relative to the Au(111) surface. Very recent STM experiments of PDI deposited Au(111) and Au(110) surfaces show similar 1D chain structures of PDI as well as the ability of CO_2 absorption to reduce repulsive inter-chain interactions and cause the chains to coalesce.[25]

As an extension to these earlier studies on PDI/Au(111), this work reports on a study of the related BPDI molecule deposited on Au(111) using variable-temperature STM measurements and DFT calculations. STM images show that BPDI also spontaneously organizes into 1-D molecular chains when vapor deposited at room temperature. The increased length of the repeating units within the BPDI chains relative to PDI matches that expected for a second phenyl ring and thereby supports a flat lying geometry for both systems. Dispersion corrected DFT-D2 calculations also provide support for the formation of BPDI-Au chains involving the insertion of Au-adatoms as the most stable surface structure. Current-imaging tunneling spectroscopy (CITS) was also used to generate 3D conductance maps that probe the local density of states along the BPDI-Au chains. The CITS measurements provide evidence for an occupied state located ~0.7 eV below the Fermi level which is spatially extended along the length of the chain.

2. Experimental and theoretical methods

STM experiments were conducted on a Createc low-temperature STM instrument at the Center for Functional Nanomaterials at Brookhaven National Laboratory. The base pressure in the STM chamber was typically lower than 5×10^{-11} Torr. The sample was cleaned and the BPDI layer deposited in a preparation chamber that could be isolated from the STM. The Au(111) crystal was cleaned by repeated cycles of Ar ion sputtering at 1 kV followed by annealing to 800 K. The clean Au(111) surface showed extended terraces with the characteristic herringbone reconstruction pattern.[26] Because the BPDI molecules have very low vapor pressure ($<10^{-4}$ Torr),

the samples were deposited onto the Au(111) surface at 300 K using a line-of-sight doser consisting of a metal tube which is connected to a glass sample reservoir via a small gate valve. The BPDI sample was kept at ~350 K during deposition. No decomposition products of BPDI were observed by a residual gas analyzer during dosing or in STM images of the surface after dosing under these conditions.

All STM images presented here were acquired at 95 K or 5 K using a tungsten tip in constant current mode. The current imaging tunneling spectroscopy (CITS) experiments were conducted at 5 K to minimize drift during the acquisition of current-voltage (*I*–*V*) curves. In CITS experiments, constant-current STM images were recorded simultaneously with *I*–*V* curves, and the feedback loop was disabled during acquisition of the spectra. The STM image and tunneling spectroscopy analyses were carried out using the GXSM software.[27,28]

DFT calculations with semi-empirical dispersion corrections in the DFT-D2 scheme[29] were carried out using the VASP package[30,31] with a plane-wave basis set ($E_{cut} = 400$ eV), GGA/PBE[32] exchange-correlation functional and projected augmented wave pseudopotentials.[33] The C_6 parameter for Au (220 eVÅ^6) was derived from a hybrid QM/MM procedure and has been demonstrated to reproduce the experimentally measured adsorption distance and energy of small aromatic molecules on Au(111).[34] The Au(111) surface is modeled by a 4-layer unreconstructed slab at the optimized bulk equilibrium lattice constant (4.14 Å).[15] The adsorption of flat lying BPDI-Au chains were studied using a surface unit cell with lattice parameters $a_1=\sqrt{31}d_{\text{Au-Au}}$ and $a_2=2\sqrt{3}d_{\text{Au-Au}}$, which are along $[6\bar{5}\bar{1}]$ and $[10\bar{1}]$ directions, respectively. Here $d_{\text{Au-Au}}$ is the Au-Au interatomic distance (2.9 Å for bulk Au). The BPDI-Au chains run straight along $\vec{a}_1$ (about 9° with respect to the $[1\bar{1}0]$ direction) with all Au-adatoms located at the *fcc* sites, corresponding to a periodicity of $L = 5.6\ d_{\text{NN}}$. Such choices of unit cell

and chain orientation were based on the experimentally observed chain periodicity and orientations. For comparison, we also examined the case in which the flat-lying BPDI molecule is adsorbed directly on Au(111) without the Au adatom. In addition, we studied the vertical adsorption of BPDI on Au(111) using a (3x3) surface unit cell. A (2×4×1) and a (3×3×1) *k*-point grids were employed for the flat-lying and vertical configurations, respectively. During structure optimization, the bottom Au layer was kept fixed while the top three Au layers and the adsorbed molecules were fully relaxed till the maximum force was smaller than 0.01 eV/Å.

We define the adsorption energy of BPDI molecules on a Au(111) surface at the presence of the adatom, E_{ad}, as

$$E_{ad} = E[\text{BPDI+adatom/Au(111)}] - (E[\text{adatom/Au(111)}] + E[\text{BPDI}]) \quad (1)$$

where the individual terms on the right hand side correspond to the total energies of the complete adsorption system, the Au(111) surface with adatom(s), and the gas-phase BPDI molecule, respectively. The adatom formation energy is not included in the above expression, which is estimated to be about 0.7 eV if the adatom is to be extracted from the bulk; that is an upper bound for various possible scenarios, e.g. adatom lifted from the reconstructed Au(111) surface or released from step edges.

3. Results and Discussion

3.1 Adsorption structures

As seen in Figure 1, the BPDI molecules are observed to self-assemble into 1-D molecular chains on the Au surface at 300 K. At this coverage (0.18 ML), the $(22 \times \sqrt{3})$ reconstruction of the Au(111) surface is still visible underneath the chains which is similar to that observed for PDI/Au(111) surfaces at comparable coverages.[25,35] The coverage was

calculated from STM images and represents the fraction of the Au(111) surface covered by the molecular chains. The 1-D chains can be seen to consist of alternating small and large features, with the latter expected to be the BPDI molecules. The line profile shown in Figure 1c for a small section of a BPDI chain (indicated by arrow in Figure 1b) yields the length of the monomer repeat unit at 16.1 ± 0.3 Å. This is longer than that observed for PDI chains on Au(111) , 11.7 ± 0.2 Å, by approximately the length of an extra phenyl ring (see Figure 3). [17,18,24] The correlation between the monomer length and molecular dimensions supports an adsorption geometry in which BPDI molecules lie parallel (or nearly so) to the surface. Since abutting -NC terminal groups are not likely to be chemically linked, diisocyanide chain formation would require a common surface binding site for both terminal –NC groups. The latter could be a surface Au atom or a Au-adatom as proposed for organic thiol/thiolate bonding on Au(111).[19] Previous DFT calculations for [-PDI-Au-] structures[18,25] have assumed the adatom binding site, which is also supported by our DFT-D2 results for [-BPDI-Au-] chains (see below). It is therefore likely that the smaller features along the chains are associated with Au-adatoms which link adjacent BPDI molecules. Our calculations (Table 1) indicate that the magnitude of the adsorption energy of a flat-lying BPDI molecule on Au(111) increases by more than 1.2 eV when the two isocyanide groups bind through Au-adatoms instead of directly to the surface. The adatom-mediated adsorption is more favorable even after considering the energetic cost of extracting an Au atom from the bulk of the substrate to form an adatom, (ΔE ~0.7 eV). The latter is expected to be an upper bound since the energy to release an adatom from steps or the Au(111) reconstruction should be significantly less than from the bulk.

Like the 1-D chains of PDI on Au(111), the BPDI chains are generally oriented along the $[1\bar{1}0]$ direction, but are less straight with small, but frequent changes in direction (± 3-11°) and

occasionally large changes (± 51°) that appear to keep the chain confined to the *fcc* regions of the Au(111) reconstruction (see Figure 1a and 2a). To understand the origin of these changes in chain direction, we performed simple geometric calculations using the periodicity of the 1D chains and the underlying Au(111) surface. Previous STM and DFT studies of PDI-Au chains suggest that the Au-adatoms are preferentially located at three-fold hollow sites.[18,25] The preferred orientations of the chains can then be calculated by considering directions that connect *fcc-fcc*, *hcp-hcp* or *fcc-hcp* three-fold hollow sites and also span the monomer repeat distance (~16 Å). The distance between *fcc-fcc* and *hcp-hcp* sites can be calculated from the expression

$$d_{ij} = d_{\mathrm{Au-Au}}\sqrt{i^2 + j^2 + ij} \tag{2}$$

in which i and j correspond to lattice vectors along the $[1\bar{1}0]$ and $[10\bar{1}]$ directions and $d_{\mathrm{Au-Au}}$ is Au-Au interatomic distance for bulk gold (2.88 Å). The analogous expression for directions connecting *fcc-hcp* three-fold hollow sites is

$$d_{ij} = d_{Au-Au}\sqrt{\left(i+\tfrac{1}{3}\right)^2 + \left(j+\tfrac{1}{3}\right)^2 + \left(i+\tfrac{1}{3}\right)\left(j+\tfrac{1}{3}\right)} \tag{3}$$

The best match to the observed monomer repeat distance for connecting *fcc-fcc* and *hcp-hcp* sites is 16.1 Å with (i,j)= (5,1), (6,-1), (6,-5) and (1,5) which translate into angular deviations from the $[1\bar{1}0]$ direction of ± 9° and ± 51°. For *fcc→hcp* sites, the best match is 15.9 Å for (i,j) = (5,0), (6,-3), (6,-4) and (0,5), corresponding to 3°, -25° ,-35° and 57°; the angles have opposite signs for *hcp→fcc* sites. The three-fold symmetries of the *fcc* and *hcp* sites mean that equivalent chain directions can be derived by adding 120° or 240°. In Figure 2 we show regions of the STM images with measured angular deviations of the molecular chains relative to the $[1\bar{1}0]$ direction. According to the derivation above, the short chain segments oriented at ± 51° in

Figure 2a are aligned along paths that connect *fcc*→*fcc* or *hcp*→*hcp* sites. These relatively large changes in direction occur when these particular chains encounter the soliton walls which mark the transition from *fcc* to *hcp* regions of the Au(111) reconstruction. The latter suggest an energy barrier for crossing the soliton walls which keeps the chains confined to the fcc regions of the reconstruction. This barrier is likely to be small as most of the other observed chains in Figure 2a cross the soliton walls without significant deflections. The three nearly parallel chains shown in Figure 2b exhibit small changes in direction that can be accounted for by the angular deviations calculated above. Specifically, most of the changes in orientation are within ± 1-2° of the predicted ± 9° deviation expected for directions connecting *fcc*-*fcc* and *hcp*-*hcp* sites. The small variations in angles from those predicted by equations (2) and (3) are likely the result of measurement uncertainty (± 1°) and variations of the substrate atom positions (lattice constant) along $[1\bar{1}0]$ direction as chains move across *fcc* and *hcp* domains of the reconstruction.[19,36] Much less frequent are deviations of ± 3° and ± 26° which can be attributed to chain directions connecting *fcc*-*hcp* sites. Overall, these observations are consistent with the structural model where Au-adatoms are incorporated into the 1D molecular chains and also suggests that preferred chain orientation is along directions that connect *fcc* or *hcp* three-fold hollow sites.

Figure 3 shows the calculated lowest energy structures of the [-BPDI-Au-] chains on Au(111) and the structural parameters are summarized in Table 1. The lateral chain separation is about 10 Å, and the chain periodicity of 16.3 Å which is consistent with the measured unit chain lengths of 16.1 ± 0.3 Å. Since the position of the Au-adatoms, and therefore the periodicity of the monomer repeating unit, are restricted by the underlying Au(111) lattice, the molecular plane is not perfectly flat. As illustrated in Figure 3b, the center of the BPDI molecule is bulged outwards away from the substrate, and the two isocyanide groups make an angle of 8° with

respect to the plane of the surface. The calculated distance between the carbon atom on the –NC group and the Au-adatom, $d_{\mathrm{Au-C}}$, is about 2.02 Å, longer than that in the case when the BPDI molecules are vertically adsorbed on the Au-adatoms ($d_{\mathrm{Au-C}}$ =1.95 Å). In addition, the Au-adatom is more loosely bound to the underlying Au(111) substrate with a height of h_{Au} = 2.58 Å to the surface, while it is much smaller when the adatom is bonded to the upright BPDI molecule (h_{Au} = 2.11 Å). Comparison of the computed adsorption energies reveal that the flat-lying adsorption of BPDI molecules linked by Au-adatoms is energetically favored over vertical adsorption structures. The large energy gain (~2 eV) in the flat 1-D chain structure can be partly attributed to the presence of two Au-CN bonds per adatom versus only one in the vertical adsorption structure. More importantly, the vdW dispersion interactions, which draw the molecule closer to the Au(111) surface, contribute significantly to the energetic stability of the former by as much as $\Delta E_{\mathrm{ad}}^{\mathrm{disp}}$=1.74 eV, whereas $\Delta E_{\mathrm{ad}}^{\mathrm{disp}}$ is only about 0.1 eV in the latter case.

Table 1 also lists the computed structure and energetics of the flat-lying BPDI molecule adsorbed directly to Au(111) in the absence of adatoms. In this case, the BPDI molecule binds to the nearest surface Au atoms, and finite Au-BPDI-Au segments are formed instead of continuous BPDI-Au chains since neighboring BPDI molecules are no longer linked by bonding to the same Au atom. The surface Au atoms that bind to BPDI are lifted up by almost 0.3 Å, accompanied by severe structural deformation of the molecule, as indicated by the large tilting angle of the NC group of 32°. Indeed the total energy of the deformed BPDI increases by about 0.7 eV compared to gas-phase. Correspondingly, the adsorption energy is lowered by 1.2 eV compared to the case of adatom-assisted adsorption, indicating much weaker binding.

3.2 Current-Imaging Tunneling Spectroscopy

The electronic structure of the BPDI-Au chains was probed by spatially-resolved tunneling spectroscopy measurements (CITS). In this experiment, the tunneling conductance (dI/dV) was measured as a function of sample bias at each point along a small segment of a BPDI-Au chain (Figure 4; top panel) to form a 3D conductance map (Figure 4; lower panel). Since dI/dV is a measure of the local density of states (LDOS), the conductance map provides a measure of the LDOS of the molecular chains convoluted with those of the Au(111) substrate below. At negative and positive sample bias, the measurement probes the occupied and unoccupied states, respectively, with zero bias corresponding to the Fermi energy (E_F).

As seen in Figure 4, the conductance across the chain at low sample bias is relatively small and featureless suggesting a low density of states in the range $E_F \pm 0.5$ eV. At somewhat more negative bias, prominent conductance maxima appear along the chain, which are centered at -0.67 V. The vertical lines from the topographical image show that small nearly circular maxima align with the presumed positions of the Au-adatoms. Regions of high conductance are also centered in the regions of the biphenyl groups of the BPDI molecules. The position of this state is similar to that found for PDI-Au chains on Au(111) using 2PPE and tunneling spectroscopy measurements (E_F - 0.88 eV).[24] The latter was only observable under conditions where the PDI-Au chains were present on the surface after deposition or annealing to room temperature, but absent when the PDI molecules were deposited at low temperatures where they formed mostly disordered molecular islands. These previous results and those in Figure 4 indicate that the low energy occupied states for PDI and BPDI on Au(111) have similar electronic character and are specific to diisocyanide-Au chain formation. The conductance map in Figure 4 also suggests the LDOS for this level is extended along the BPDI-Au chain axis that could result from electron conjugation with the π-derived orbitals of the biphenyl groups.

At bias voltages below -1.2 V, conductance minima are seen to develop near at the Au-adatom positions and in the regions of the phenyl groups, while maxima start to form in the regions expected for the isocyanide groups. Maxima localized in the regions of the isocyanide groups also begin to develop at positive bias voltages above +0.9 V. These isocyanide derived states at both higher positive and negative bias are less extended along the chain, with significantly smaller LDOS at the Au-adatom and phenyl ring positions than the state feature at -0.67 V. It is likely that these levels are derived from the HOMO and LUMO levels of BPDI which are hybridized and lowered in energy through interactions with the Au(111) substrate and Au-adatoms.

The main result of the CITS measurements is the observation of a BPDI-Au chain-derived occupied state with conductance maxima at -0.67 V that extend across the length of the chain. This state lies in the expected HOMO-LUMO gap of BPDI on Au(111) (> 6 eV)[13] and thereby represents an interfacial state that is not readily accounted for by simple energy shifts of the molecular orbitals or hybridization with the Au(111) substrate.[37,38] Moreover, this occupied state is unlikely to be associated with the Au(111) surface Shockley state, as our previous 2PPE study of PDI-Au chains on Au(111) showed that the surface state is quenched at PDI coverages of ~0.5 ML.[24] Other studies have also shown that adsorbates generally move the Shockley state up in energy and even above E_F for strongly interacting organic systems.[39-43] Interfacial states have also been shown to originate from LUMO levels that are shifted below E_F due to strong interactions with the Au(111) surface. Such a LUMO-derived occupied state has been identified by photoemission for PTCDA adsorbed on Ag(110) at (E_F - 0.7 eV)[35] and Au(111) at (E_F - 0.3 eV).[38,41] The larger HOMO-LUMO gap expected for BPDI compared to PTCDA makes

such a LUMO shift less likely, but will strongly depend on the alignment of the LUMO orbitals relative to E_F.

4. Summary

BPDI molecules vapor deposited on Au(111) at room temperature self-assemble into 1-D chains which grow preferentially along the $[1\bar{1}0]$ direction of the Au(111) surface. The observed periodicity of the chains (16.1 ± 0.3 Å) is consistent with a structural model in which the BPDI molecules lie parallel to the surface and are interconnected by Au-adatoms. Compared to the PDI-Au chains studied earlier, the BPDI-Au chains exhibit deviations from linearity along directions that connect *fcc* or *hcp* sites separated by the periodicity of the chain. DFT calculations including dispersion contributions (DFT-D2) show that Au-adatom binding of the BPDI in a flat-lying geometry is energetically favored over binding to Au surface atoms or upright binding to a Au-adatom with one free –NC group. Spatially-resolved differential conductance measurements reveal a state at -0.67 V below E_F, with maxima that are located at the positions of the Au-adatoms and the biphenyl rings of BPDI molecules. This state is similar in energy to a feature observed in the 2PPE and STS spectra of PDI-Au chains and is attributed to a chain-derived interface state. The electronic origin of this state will be the subject of future theoretical studies employing higher level of theory such as the GW method which provide a more accurate description of interface energy level alignment[16].

The ability to self-organize as flexible 1-D molecular chains with Au-adatoms suggest that diisocyanides with various backbone structures may offer unique opportunities for use in nanoscale electronic applications, e.g., as molecular "interconnects." By comparison, vapor deposited thiols (R-SH) or dithiols (HS-R-SH) self-assemble as R-S-Au-S-R dimers on the Au(111) surface, with larger scale organization ("striped" phases) driven by intermolecular

interactions that do not chemically interconnect the individual dimers. On the other hand, longer diisocyanide molecules, such as long-chain alkyl or aryl molecules, may be able to self-assemble into molecular chains similar to PDI or BPDI, provided that the molecular length is commensurate with (multiple) periodicity of Au(111). The spatial delocalization of the low energy state near -0.7 eV in BPDI suggests that conjugation along the length of the molecular chains may be possible by appropriate choice of aromatic substitution to produce molecular "wires" appropriate for hole transport. In this context, the interface state observed here would offer a significantly lower barrier (~0.7 eV) to hole conduction than the HOMO-derived level of BPDI/Au(111) which is estimated to be at least 3 eV below E_F.[13] Additional design flexibility could include self-assembly of diisocyanides on other metal surfaces, e.g., Cu surfaces where Cu-adatom formation is also known to result in the presence strongly interacting adsorbates.

Acknowledgements

The authors would like to thank Dr. Sally Swanson (IBM) for providing the BPDI sample. Work performed by JZ and MGW in the Chemistry Department at Brookhaven National Laboratory was supported by the U.S. Department of Energy, Office of Basic Energy Sciences, under Contract No. DE-AC02-98CH10086. STM measurements and calculations were carried out at the Center for Functional Nanomaterials at Brookhaven National Laboratory, which is supported by the U.S. Department of Energy, Office of Basic Energy Sciences, under Contract No. DE-AC02-98CH10886.

References

(1) Schreiber, F. *Prog. Surf. Sci.* **2000**, *65*, 151.

(2) Love, J. C.; Estroff, L. A.; Kriebel, J. K.; Nuzzo, R. G.; Whitesides, G. M. *Chem. Rev.* **2005**, *105*, 1103.

(3) Kind, M.; Wöll, C. *Prog. Surf. Sci.* **2009**, *84*, 230.

(4) Chen, J.; Calvet, L. C.; Reed, M. A.; Carr, D. W.; Grubisha, D. S.; Bennett, D. W. *Chem. Phys. Lett.* **1999**, *313*, 741.

(5) Chen, J.; Wang, W.; Klemic, J.; Reed, M. A.; Axelrod, B. W.; Kaschak, D. M.; Rawlett, A. M.; Price, D. W.; Dirk, S. M.; Tour, J. M.; Grubisha, D. S.; Bennett, D. W. *Ann. N.Y. Acad. Sci.* **2002**, *960*, 69.

(6) Hong, S.; Reifenberger, R.; Tian, W.; Datta, S.; Henderson, J. I.; Kubiak, C. P. *Superlattices Microstruct.* **2000**, *28*, 289.

(7) Henderson, J. I., Feng, S., Bein, T., Kubiak, C.P. *Langmuir* **2000**, *16*, 6183.

(8) Chu, C.; Ayres, J. A.; Stefanescu, D. M.; Walker, B. R.; Gorman, C. B.; Parsons, G. N. *J. Phys. Chem. C* **2007**, *111*, 8080.

(9) Seminario, J. M.; De la Cruz, C. E.; Derosa, P. A. *J. Am. Chem. Soc.* **2001**, *123*, 5616.

(10) Dahlke, R.; Schollwöck, U. *Phys. Rev. B* **2004**, *69*, 085324.

(11) Xue, Y.; Ratner, M. A. *Phys. Rev. B* **2004**, *70*, 205416.

(12) Bai, P.; Li, E.; Neerja; P. Collier, P. *Nanotechnology, IEEE Transactions on* **2005**, *4*, 422.

(13) Caruso, A. N.; Rajesh, R.; Gallup, G.; Redepenning, J.; Dowben, P. A. *J. Phys. Chem. B* **2004**, *108*, 6910.

(14) Kim; Beebe, J. M.; Jun, Y.; Zhu, X. Y.; Frisbie, C. D. *J. Am. Chem. Soc.* **2006**, *128*, 4970.

(15) Li, Y.; Lu, D. Y.; Swanson, S. A.; Scott, J. C.; Galli, G. *J. Phys. Chem. C* **2008**, *112*, 6413.

(16) Li, Y.; Lu, D.; Galli, G. *J. Chem. Theory Comput.* **2009**, *5*, 881.

(17) Boscoboinik, J. A.; Calaza, F. C.; Habeeb, Z.; Bennett, D. W.; Stacchiola, D. J.; Purino, M. A.; Tysoe, W. T. *Phys. Chem. Chem. Phys.* **2010**, *12*, 11624.

(18) Boscoboinik, J.; Kestell, J.; Garvey, M.; Weinert, M.; Tysoe, W. T. *Top. Catal.* **2011**, *54*, 20.

(19) Maksymovych, P.; Voznyy, O.; Dougherty, D. B.; Sorescu, D. C.; Yates, J. T. *Prog. Surf. Sci.* **2010**, *85*, 206.

(20) Fan, X.; Zhang, C.; Liu, Y.; Lau, W. M. *J. Phys. Chem. C* **2012**, *116*, 19909.

(21) Sharif, A. M.; Buckley, D. N.; Buck, M.; Silien, C. *J. Phys. Chem. C* **2011**, *115*, 21800.

(22) Ferrighi, L.; Pan, Y.-x.; Grönbeck, H.; Hammer, B. *J. Phys. Chem. C* **2012**, *116*, 7374.

(23) Luque, N. B.; Santos, E.; Andres, J.; Tielens, F. *Langmuir* **2011**, *27*, 14514.

(24) Zhou, J.; Acharya, D.; Camillone, N.; Sutter, P.; White, M. G. *J. Phys. Chem. C* **2011**, *115*, 21151.

(25) Feng, M.; Sun, H.; Zhao, J.; Petek, H. *ACS Nano* **2014**, *8*, 8644.

(26) Wöll, C.; Chiang, S.; Wilson, R. J.; Lippel, P. H. *Phys. Rev. B* **1989**, *39*, 7988.

(27) Zahl, P.; Bierkandt, M.; Schroder, S.; Klust, A. *Rev. Sci. Instrum.* **2003**, *74*, 1222.

(28) Zahl, P.; Wagner, T.; Moller, R.; Klust, A. *J. Vac. Sci. Technol., B* **2010**, *28*, C4E39.

(29) Grimme, S. *J. Comput. Chem.* **2006**, *27*, 1787.

(30) Kresse, G.; Hafner, J. *Phys. Rev. B* **1994**, *49*, 14251.

(31) Giannozzi, P.; Baroni, S.; Bonini, N.; Calandra, M.; Car, R.; Cavazzoni, C.; Ceresoli, D.; Chiarotti, G. L.; Cococcioni, M.; Dabo, I.; Dal Corso, A.; de Gironcoli, S.; Fabris, S.; Fratesi, G.; Gebauer, R.; Gerstmann, U.; Gougoussis, C.; Kokalj, A.; Lazzeri, M.; Martin-Samos, L.; Marzari, N.; Mauri, F.; Mazzarello, R.; Paolini, S.; Pasquarello, A.; Paulatto, L.; Sbraccia, C.; Scandolo, S.; Sclauzero, G.; Seitsonen, A. P.; Smogunov, A.; Umari, P.; Wentzcovitch, R. M. *J. Phys.-Condes. Matter* **2009**, *21*, 395502.

(32) Perdew, J. P.; Burke, K.; Ernzerhof, M. *Phys. Rev. Lett.* **1996**, *77*, 3865.

(33) Blöchl, P. E. *Phys. Rev. B* **1994**, *50*, 17953.

(34) Tonigold, K.; Groß, A. *J. Chem. Phys.* **2010**, *132*, 224701.

(35) Zou, Y.; Kilian, L.; Schöll, A.; Schmidt, T.; Fink, R.; Umbach, E. *Surf. Sci.* **2006**, *600*, 1240.

(36) Barth, J. V.; Brune, H.; Ertl, G.; Behm, R. J. *Phys. Rev. B* **1990**, *42*, 9307.

(37) Yamane, H.; Kanai, K.; Ouchi, Y.; Ueno, N.; Seki, K. *J. Electron. Spectrosc. Relat. Phenom.* **2009**, *174*, 28.

(38) Matthew, S. D.; Mats, P. *New J. Phys.* **2010**, *12*, 063014.

(39) Andreev, T.; Barke, I.; Hövel, H. *Phys. Rev. B* **2004**, *70*, 205426.

(40) Forster, F.; Hüfner, S.; Reinert, F. *J. Phys. Chem. B* **2004**, *108*, 14692.

(41) Temirov, R.; Soubatch, S.; Luican, A.; Tautz, F. S. *Nature* **2006**, *444*, 350.

(42) Sebastian, H.; Ying, L.; Rainer, H.; Martin, W.; Petra, T. *New J. Phys.* **2010**, *12*, 125022.

(43) Marks, M.; Zaitsev, N. L.; Schmidt, B.; Schwalb, C. H.; Schöll, A.; Nechaev, I. A.; Echenique, P. M.; Chulkov, E. V.; Höfer, U. *Phys. Rev. B* **2011**, *84*, 081301.

Table 1: Equilibrium structures and adsorption energy of BPDI on Au(111) in the flat-lying and vertical adsorption configuration. Two types of binding sites, surface Au atom and Au adatom, are considered. The tilt angle of N-C bond from the surface is given by $\theta_{\text{N-C}}$. h_{mol} is the averaged height of aromatic ring carbon atoms of BPDI measured from the clean Au(111) surface, and h_{Au} is that of the Au adatom or surface atom bonded to BPDI. E_{ad} and $\Delta E_{\text{ad}}^{\text{disp}}$ are the adsorption energy and its contribution from vdW dispersion interactions.

Adsorption geometry	Site	$d_{\text{N-C}}$ (Å)	$d_{\text{Au-C}}$ (Å)	$\theta_{\text{N-C}}$ (°)	h_{mol} (Å)	h_{Au} (Å)	E_{ad} (eV)	$\Delta E_{\text{ad}}^{\text{disp}}$ (eV)
Flat-lying	surface atom	1.19	2.10	32.4	3.20	0.26	2.23	1.90
	adatom	1.18	2.02	8.0	3.17	2.58	3.46	1.74
Vertical	surface atom	1.18, 1.19	2.02	90	-	0.06	0.84	0.34
	adatom	1.18, 1.19	1.95	90	-	2.11	1.43	0.10

Figure Captions

Figure 1: STM images of BPDI on Au(111) dosed at 300 K at a coverage of 0.18 ML: (a) image size: 50 × 50 nm; V= -1.6 V, I = 0.15 nA; (b) image size: 29×29 nm, V = -1.6 V, I = 0.2 nA; (c) height profile of the BPDI molecular chain along the red arrow shown in (c). STM measurements were taken at 95 K.

Figure 2: STM images of BPDI molecular chains on Au(111) along with measured angular deviations relative to the $[1\bar{1}0]$ direction: (a) image size: 20 × 20 nm; V= -1.6 V, I = 0.15 nA; (b) image size: 29×29 nm, V = -1.6 V, I = 0.2 nA. The BPDI coverage is 0.18 ML and the STM measurements were taken at 95 K.

Figure 3: Top and side views of DFT-optimized BPDI-Au chains on Au(111) in the ($\sqrt{31} \times 2\sqrt{3}$) unit cell.

Figure 4: Conductance (dI/dV) map as a function of energy and position along selected line on BPDI-Au chain on Au(111) surface deposited at 300 K: (top) constant-current image of the BPDI-Au chain, V = -1.6 V, I = 0.15 nA (bottom) dI/dV along the line shown in the topographical image. The color bar indicates the relative magnitude of the differential tunnel conductance. The dotted lines provide reference points along the scan line between the topographical image and conductance map. Conductance data acquired at 5 K.

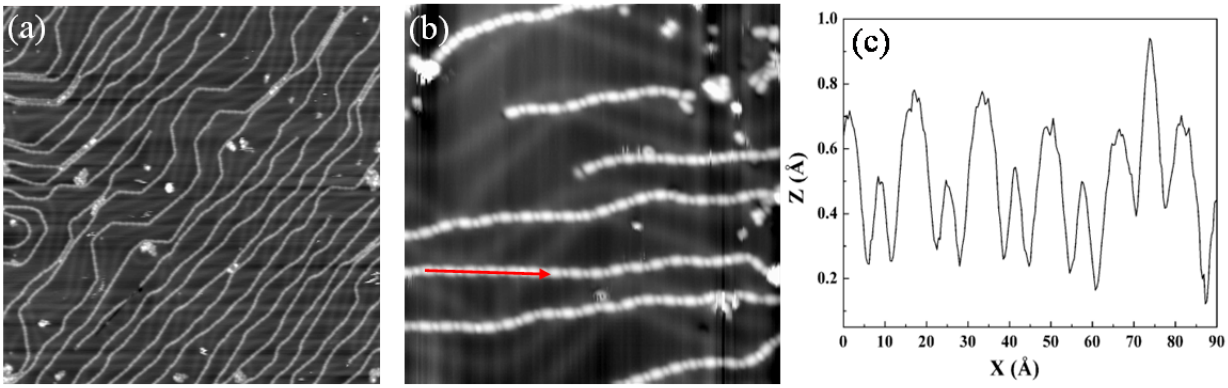

Figure 1

.

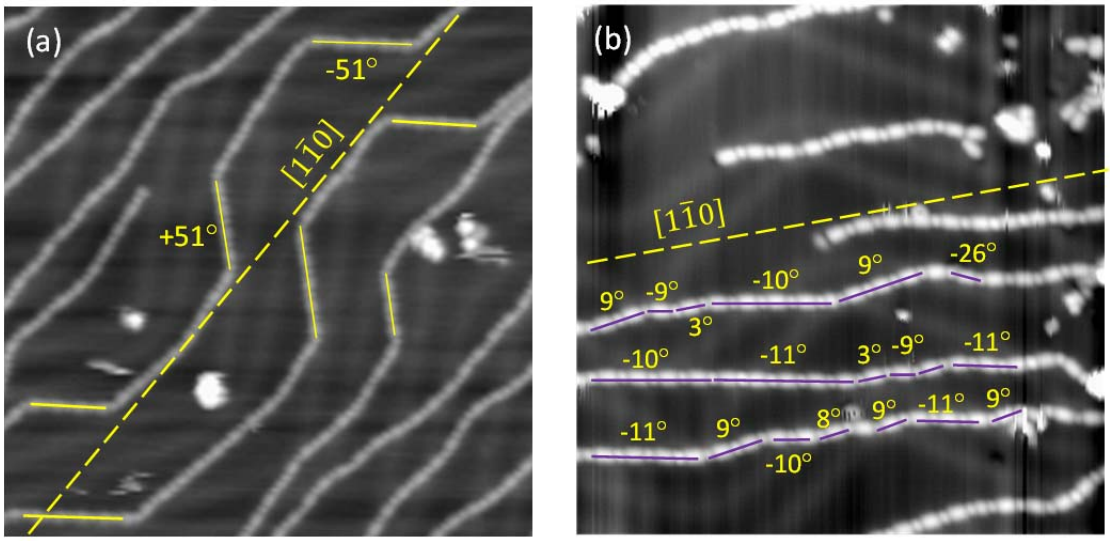

Figure 2

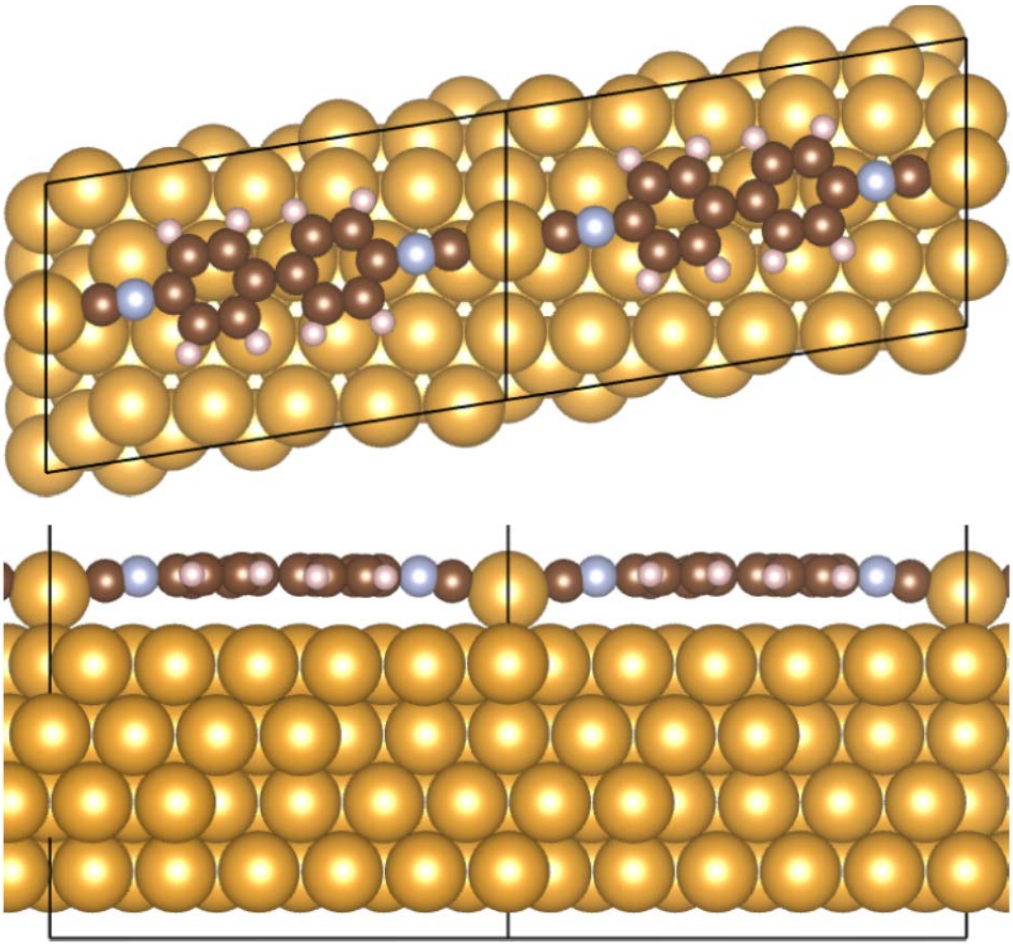

Figure 3

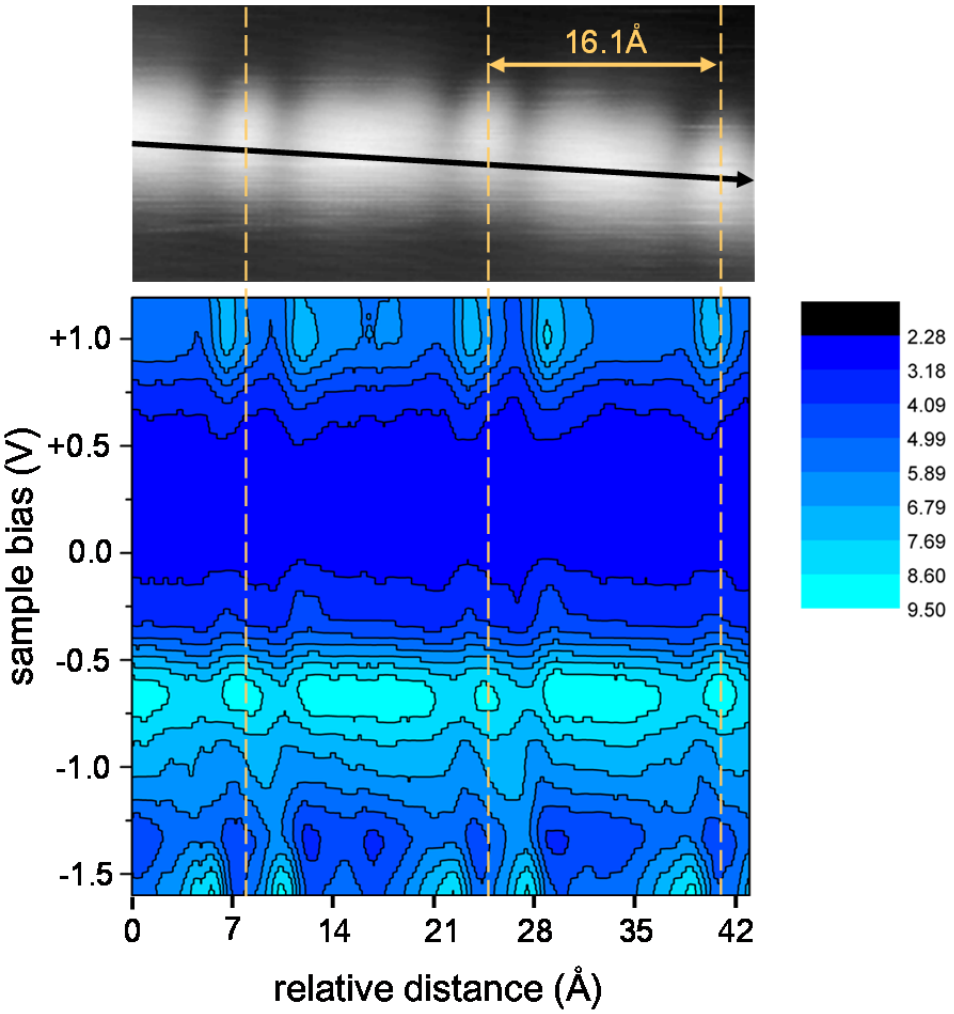
16.1Å
+1.0
+0.5
0.0
-0.5
-1.0
-1.5
sample bias (V)
0
7
14
21
28
35
42
relative distance (Å)
2.28
3.18
4.09
4.99
5.89
6.79
7.69
8.60
9.50

Figure 4